Automation of Surgical Instruments for Robotic Surgery: Automated Suturing Using the EndoStitch Forceps

Original Scientific Paper

Omaira Tapias*
Popular University of Cesar, Faculty of Engineering,
Valledupar, Cesar, 200003, Colombia,
omairatapias@unicesar.edu.co

Andrés Vivas
University of Cauca,
Popáyan, Cauca, 190003, Colombia,
avivas@unicauca.edu.co

Juan Carlos Fraile
University of Valladolid,
Valladolid, 47011, Spain,
jcfraile@uva.es

*Corresponding author

Abstract *– Suturing in minimally invasive robotic surgery poses significant challenges in terms of technique, du- ration, and tool usage. This study presents an innovative semi-autonomous robotic system for suture automation in minimally invasive surgery. The system integrates motorized EndoStitch forceps with a UR3 collaborative robot, combining robotic dexterity with the functionality of a proven surgical tool. The de- sign of the motorized gripper coupling, the development of a modular ROS-based control architecture, and the implementation of a library of parameterized movements optimized for suturing are described. Exper- imental results, obtained in tissue simulations, demonstrate micrometer accuracy in needle positioning. The variability of the positioning error and its relation to the characteristics of the surgical environment are analyzed. This system represents a representative advance towards reducing the surgeon's cognitive load, improving accuracy and efficiency in robotic suturing, and opening new avenues for safer and more consistent surgical procedures. The semi-autonomous robotic suturing system demonstrated micrometer- level precision in tests. Mean positioning errors ranged from* 0.5×10^{-5} *m to* 2.0×10^{-5} *m, with low standard deviations (highest at* 0.70×10^{-5} *m) indicating high repeatability.*

Keywords: *Robotic Suturing, Surgical Automation, EndoStitch Forceps, UR3 Collaborative Robot, Minimally Invasive Surgery, Semi-Autonomous Suturing*

Received: Received: March 21, 2025; Received in revised form: June 24, 2025; Accepted: June 25, 2025

1. INTRODUCTION

Minimally invasive surgery (MIS) has revolu- tionized modern medicine, offering patients faster recovery times and reduced scarring compared to traditional open procedures. Despite these ad- vances, certain maneuvers, such as suturing, re- main particularly challenging due to the dexter- ity, precision, and time they demand, especially in the context of robotic surgery where, although er- gonomics and vision are improved, teleoperation of complex sutures remains a demanding task. To address these limitations, the automation of surgi- cal instruments is emerging as a promising field, seeking to improve efficiency, consistency, and safety in the operating room. In this context, the EndoStitch forceps, a tool widely used and proven in laparoscopic surgery for its ingenious needle- passing mechanism, presents an excellent oppor- tunity for automation.

While robotic surgery has enabled many ad- vances, studies such as [1] indicate that robotic consoles can be mentally demanding for novice surgeons, requiring formal training. Challenges persist, such as ergonomics, training optimization, and cost-benefit evaluation. Therefore, research is justified in adapting and automat-

ing specialized forceps that can improve not only the procedure itself but also the surgeon's work [2],[3][4].

This work presents an innovative semiautonomous robotic system for suture automation in MIS. The system integrates a motorized EndoS- titch forceps, whose needle manipulation mecha- nism has been motorized, with a UR3 collabora- tive robot. The main objective is to develop a sys- tem capable of performing sutures with high pre- cision and repeatability, reducing human variabil- ity and improving efficiency in minimally invasive suturing procedures. The design of the motorized forceps coupling, the development of a modu- lar ROS-based control architecture, and the imple- mentation of a library of parameterized movements optimized for suturing are described.

The **main contributions** of this work include:

- A semi-autonomous robotic system for automated suturing, integrating an EndoStitch forceps with a motorized actuation mechanism and a collaborative robot, enabling automatic needle passing between its jaws.
- The potential improvement in suturing precision and consistency, which could translate to reduced human variability and optimized surgical time, thereby decreasing the surgeon's cognitive load by allowing them to focus on higher-level aspects of the intervention.
- A modular and adaptable ROS-based control platform with a library of parameterized movements, demonstrating the concept's viability with micrometer-level precision in simulators and facilitating future research and the integration of advanced functionalities such as vision guidance.

This paper is organized as follows: Section 2 (Methodology) details the methodologies employed, including the finite element simulation of the needle-tissue interaction, the description of the robotic platform (UR3 robot and motorized EndoStitch forceps), and the ROS-based software control architecture. Section 3 (Results) presents the experimental results of the system's evaluation in a simulated environment, analyzing positioning accuracy. Section 4 (Discussion) discusses the findings, study limitations, and implications of the work in the field of surgical automation. Finally, Section 5 (Conclusion) concludes the paper by summarizing the main contributions and outlin- ing future research directions.

1.1. INTERACTION MODEL BETWEEN STRAIGHT NEEDLE AND TISSUE IN SUTURING

Modeling the interaction between a straight needle and biological tissue is a critical aspect in the design and optimization of suturing procedures, particularly within the context of automated suturing performed by robotic systems employing EndoStitch-type forceps tools.

The intrinsic properties of the tissue, such as its elasticity, viscoelasticity, and stress-strain behavior, are determinant factors in the biological material's response to straight needle insertion. These properties, which can vary considerably among different tissue types and even within the same tissue (exhibiting heterogeneity and anisotropy), dictate how the tissue deforms, resists penetration, and recovers its original shape, thereby directly influencing the interaction forces.

1.1.1. Force analysis in linear needle penetration

For the specific case of linear penetration, as executed by a straight needle, the force analysis focuses on identifying and quantifying the components that oppose the needle's advancement. Cheng et al. [5] propose a model where the primary force restricting needle penetration is damped viscous friction. This force is a function of penetration velocity and is influenced by both static and kinetic friction.

The proposed friction force model is initially decomposed into static and kinetic friction components, as shown in Equation (1):

$$f_{friccion}(v, z) = f_s(z) + f_k(v, z) = \mu_s N + \mu_k N \quad (1)$$

Where:

- $f_{friccion}(v, z)$ is the total friction force, dependent on the penetration velocity v and insertion depth z.
- $f_s(z)$ is the static friction component, which must be overcome to initiate or continue motion at low velocities.
- $f_k(v, z)$ is the kinetic friction component, active once the needle is in motion.
- μ_s and μ_k are the static and kinetic friction coefficients, respectively, which depend on the properties of the needle-tissue interface.
- N is the normal force acting on the needle shaft, perpendicular to the penetration direction. This normal force is generated by the compression and displacement of the tissue surrounding the needle.

To more explicitly incorporate the dependence on penetration velocity, the model is refined as shown in Equation (2):

$$f_{friccion}(v, z) = (\mu_s + \eta_v)N \quad (2)$$

In this formulation, η represents a viscous damping constant, which models how frictional resistance increases with penetration velocity v.

While the cutting force ($F_{cutting}$) exerted by the sharp needle tip to initiate tissue separation is crucial, especially at the onset of penetration, the model by Cheng et al. [5] emphasizes the dominant contribution of friction forces along the needle shaft once it has penetrated to a certain depth. Unlike curved needles, where a sweeping force (F_{sweep}) can arise due to internal tissue compres- sion from the circular motion, this effect is

less pronounced in the linear penetration of a straight needle, or it manifests primarily as the normal force N that contributes to friction. Developing sensors capable of detecting the contact force of a needle presents a significant technical challenge; however, recent research has explored the use of piezoelectric materials in the surgical field for this purpose [6], [7], [4] .

Currently, commercially available sensors suit- able for placement on surgical needles are lacking due to constraints related to size and integration with surgical tools. Therefore, this work presents a simulation developed in Ansys to analyze this aspect.

1.2. RELATED WORK

The automation of surgical instruments in robotic surgery has experienced a significant surge in recent years, driven by the pursuit of more precise, efficient, and less invasive procedures. Various studies have addressed the motorization of existing surgical instruments and their integration with robotic platforms, with the aim of reducing human variability and improving clinical outcomes. In the specific context of suturing, a fundamental task in numerous surgical interventions, different approaches have been explored to automate the process, from fully autonomous systems to semiautomatic solutions that assist the surgeon in specific tasks.

The following describes some relevant works that address similar aspects:

The study presented in [8] investigates the automation of a suturing device for minimally invasive surgery, based on the EndoStitch, optimizing it with a DC motor controlled by a button to allow for single-handed suturing (see Fig. 1 (c)). The conventional EndoStitch was compared to the automated version in an experiment with 20 surgeons of varying levels of laparoscopic experience, measuring suturing time and accuracy.

While in [8] they also automated the EndoStitch forceps, their approach was limited to a motorized drive with manual control (button) to facilitate single-handed suturing. Unlike their design, our work extends the automation of the EndoStitch by integrating it with a collaborative robot, opening the door to more precise and programmable control of the suturing process.

In the work by [9], a suturing robot for singleport microsurgical endoscopic surgery is presented, focused on a flexible instrument with a suturing probe and a custom joint, along with a novel mechanism for needle driving and locking. For its teleoperated control, the robot's kinematics are provided. Continuous stitch and knotting experiments prove the robot's feasibility in confined spaces; however, the limited ability to suture certain wound orientations, the needle size, the ma- neuverability in confined spaces, and the thread gripping properties impose limitations. The instrument is based on the EndoStitch forceps but adds three degrees of freedom to the end effector. Unlike the present work, the instrument they use is not yet commercially available (see Fig. 1 (d)).

In the work presented in [10], a platform was developed that combines the real handle of the instrument with a three-dimensional simulation of its tip, allowing the user to practice needle transfer and thread handling. The simulation demonstrated that the current EndoStitch interface can be difficult to master and that its automation could facilitate learning and use in minimally invasive surgery, reducing errors and training times. Unlike our work, they present a completely automated procedure.

The work by [11] presents an autonomous la- paroscopic robotic system for suturing (STAR), with the motorization of the Endo 360 tool (see Fig. 1 (a)). A segmented suturing planning strategy is proposed based on point clouds obtained from the 3D endoscope, calculating the locations of the suture points based on the coordinates of the incision groove and the cut. The consistency of the bite size obtained by STAR matches that obtained by manual suturing; however, the execution time to complete the suturing process is longer compared to manual intervention. The limitations of the system include the limited speed of the motors, the use of static endoscopic images for suturing trajectory planning, and possible disturbances in the tissue. Unlike the present work, they created the motorized adapter for another forceps, the Endo 360.

In the field of automated suturing, multiple methods have been investigated to determine the points to enter and exit the needle, including: Ink marking [12], [13], [14], the incorporation of a 3D environment with a haptic interface [15], [16], [17], the location of the desired point through teleoperated control of the instrumentation [18], wound texture analysis [19], and the analysis of wound point clouds to define the stitch position [11]. In this study, it was decided to start with direct mark- ing on the target and calibration using the robot.

Considering the above paragraphs, an alterna- tive for suture automation is proposed: a motorized coupling was developed that allows for automatic actuation of the jaws of the EndoStitch forceps. The design of this coupling integrates electronic and mechanical components that transmit movement from a motor to the jaws of the forceps, controlling the opening and closing for gripping the needle and passing the thread. The robustness and precision of this coupling are fundamental in ensuring the reliability and safety of the system. The design of the coupling was addressed in a previous publication [20] (see Fig. 1 (b)). The platform is based on a modular architecture that includes: a software block for system configura- tion, a library of adaptable movements for specific suturing tasks, a mechanism for determining the coordinates of the workspace, management of motion commands for the robot, and behavior of the forceps. The system was evaluated by performing sutures in a simulated scenario, using a silicone pad that simulates human tissue.

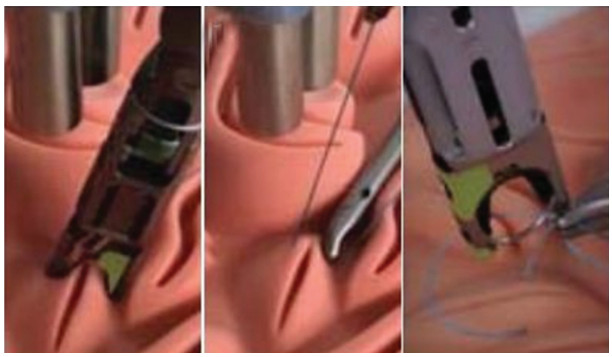

(a)

(b)

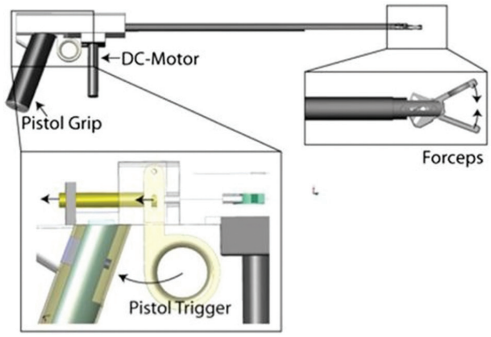

(c)

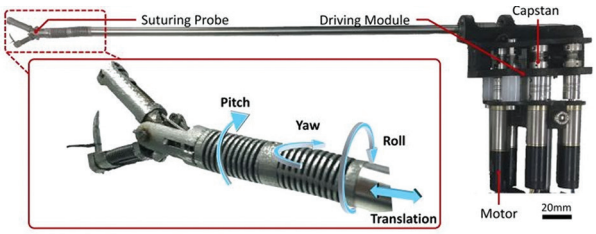

(d)

Fig. 1. Related Projects: Start automatic suturing system [11] (**a**), Endostitch adapter design [20] (**b**), EndoStitch with motorized handle [8] (**c**), Robot for single-port surgery [9] (**d**)

2. METHODS

This section outlines the methodologies em- ployed in the development and evaluation of the proposed semiautonomous robotic suturing system. To provide a foundational understanding of the mechanical interactions involved, we first present a finite element simulation analyzing the forces between the surgical needle and the tis- sue during penetration. This simulation addresses the challenge of directly measuring these forces at the tip of the needle due to sensor limitations. Following this, the subsequent subsections detail the development, implementation, and experimental evaluation of the robotic system itself.

The core of this study involves a semiautonomous robotic system designed for the automation of surgical suturing. This system integrates custom-motorized EndoStitch forceps with a UR3 robotic arm, with the goal of improving precision, repeatability, and efficiency in minimally invasive procedures. The collaborative robot UR3 (Universal Robots, Odense, Denmark) was selected as the central manipulation platform. This 6-degrees-of-freedom (DOF) robot offers a nominal payload of 3 kg, a maximum reach of 500 mm, and a declared positional repeatability of ±0.1 mm. The selection of the UR3 was based on its combination of flexibility, precision, compact size, and ease of programming, deeming it appropriate for the delicate manipulation and precise positioning required in surgical suturing tasks.

2.1. FINITE ELEMENT SIMULATION

Given the absence of sensors that can be placed at the needle tip, a simulation study of the needle-tissue interaction forces were conducted. Among the constitutive models for finite element analysis of soft tissues, a simulation was performed using ANSYS software due to its explicit dynamics capabilities, which allow for the analysis of puncture and penetration effects generated by the needle on the tissue. The environment configu- ration utilized results from Mahmud et al. [21], who analyzed skin properties, determining the following values for the Ogden model terms: μ_p = 110 Pa and α_p = 26. Based on the properties of skin components, parameters for the skin and muscle mod-els were selected as shown in Table 1. The definition of tissue characteristics, including its type and thickness, is fundamental, as the combination of these factors affect the tissue's response to needle penetration.

Table 1. Parameters for the model

Tissue	Model	Parameters
Skin	Ogden	$\mu = 110$ Pa
Muscle	Mooney-Rivlin	$\alpha = 26$ $C_{10} = 30000$ Pa $C_{01} = 30000$ Pa $d = 3.33 \times 10^{-5}$ Pa^{-1}

Fig. 2 illustrates the movement sequence developed over 10 seconds, showing the corresponding deformation and applied force indication. The simulation focuses on the corner of the simulated tissue, reflecting the common use of EndoStitch forceps for passing the needle at the tissue edge to close wounds or join tissues.

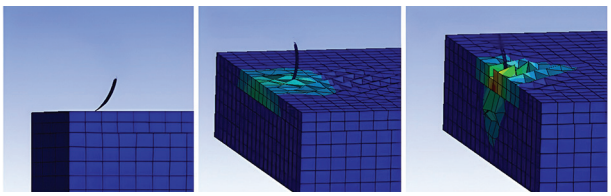

Fig. 2. Sequence of the needle penetration simulation

In the developed simulation, the equivalent stress between the bodies at the moment of contact was evaluated. Fig. 3 shows the curve representing the pressure found between the bodies.

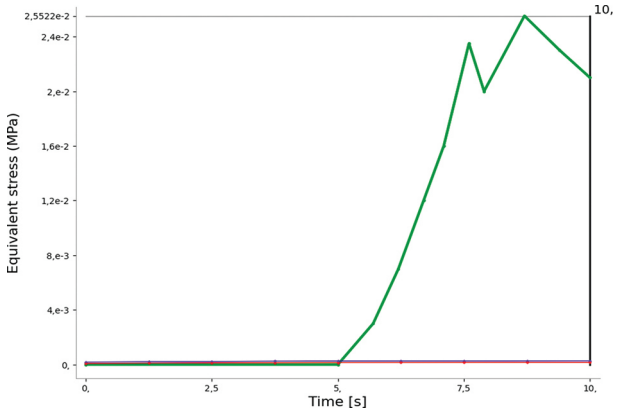

Fig. 3. Equivalent stress response

The finite element simulation provides a detailed visualization of the needle-tissue interaction during penetration, as observed in Fig. 2. This sequence illustrates the progressive stages of needle insertion: from initial contact (left), through partial penetration with visible tissue deformation and stress distribution (center), to deeper penetration where stress concentrations are more evident and extensive around the needle (right). The temporal evolution of mechanical stress in the tissue is quantified by the equivalent (von Mises) stress curve as a function of time, presented in Fig. 3. Initially, between 0 and approximately 5 seconds, the stress is minimal, corresponding to the approach or superficial contact phase of the needle. Subsequently, a gradual increase in stress is observed up to 7.5 seconds, followed by a more pronounced rise, reaching a peak of approximately 0.0255 MPa near 9.5 seconds. This peak coincides with the phase of greatest tissue penetration and deformation. Although equivalent stress is a scalar measure of the stress state intensity at a point and not the direct vectorial interaction force, its magnitude and temporal evolution are intrinsically proportional to the resistance the tissue offers to penetration. Higher equivalent stress in the tissue implies that it is exerting a greater reaction force on the needle. Therefore, this curve is fun- damental for identifying critical loading points dur- ing suturing, estimating the maximum forces the robotic system must be capable of applying, controlling, and predicting regions of high-stress concentration that could lead to tissue damage if certain thresholds are exceeded.

2.2. ROBOTIC PLATFORM: UR3 COLLABORA- TIVE ROBOT

A commercial EndoStitch forceps (Autosuture EndoStitch®, Medtronic) was modified through the design, manufacture, and integration of a specific motorized coupling. This coupling allows for automatic actuation of the jaws of the forceps, eliminating the need for direct manual intervention during the suturing process. The design of the coupling was carried out in CAD software (SolidWorks 2020, Dassault Syste`mes) and manufactured using 3D printing techniques.

For the actuation of the EndoStitch forceps, two types of servomotors were selected: an SG90, with a torque of 1.6 kg/cm (0.15 Nm), to control the needle transfer, and an MG995, with a torque of 8.5 kg/cm (0.83 Nm), to manage the opening and closing of the forceps. The choice of the SG90 for needle transfer is based on its compact size and sufficient torque to overcome the mechanical resistance associated with this process, minimizing the additional weight on the robot. The additional hardware consisted of a coupling structure manufactured using 3D printing, utilizing a rigid and lightweight plastic material to ensure structural integrity without overloading the UR3 robot. An Arduino controller was used to manage the servomotors, allowing for the programming of precise and coordinated movements, as well as communication with the robot through ROS (Robot Operating System). This configuration allowed for the integration of the forceps controls with the robot control, facilitating the execution of automatic suturing tasks and the collection of system performance data in real-time.

The design of the actuation system is based on the conversion of the rotational movement of the servomotors into the linear movement necessary to control the EndoStitch forceps. For opening and closing the forceps, the MG995 servomotor actuates a system of connecting rods connected to the handles of the forceps. This mechanism transforms the rotation of the motor into a linear displacement of the handles, allowing the forcep jaws to be opened or closed as needed to grasp the tissue. For needle transfer, the SG90 servo- motor actuates a lever that activates the internal mechanism of the forceps responsible for releas- ing the needle from one jaw and positioning it in the other. The precision of the movement in both mechanisms is controlled by the detailed programming of the servomotor angles, allowing for controlled and efficient manipulation of the forceps to perform suturing tasks with precision [20].

To ensure compatibility and optimal function- ality with the EndoStitch™ forceps, V-Loc™ 180 non-absorbable reloads were used. These reloads consist of a barbed monofilament thread, designed to provide continuous and secure tissue approxi- mation without the need for surgical knots. The needle at one end of the V-Loc™ 180 thread facilitates penetration and pas-

sage through the tissue, while the loop at the other end allows for a secure initial anchorage, simplifying and speeding up the suturing process. This choice not only guarantees the correct functionality of the forceps but also takes advantage of the benefits of a self-retaining thread, potentially reducing operating time and improving clinical outcomes.

2.3. SOFTWARE CONTROL ARCHITECTURE

The control software for the robotic system was developed using the Robot Operating System (ROS) framework, specifically the Melodic Morenia distribution, running on an Ubuntu 18.04 LTS environment. The software architecture is based on a modular structure, which facilitates the develop- ment, debugging, and maintenance of the system. This architecture is depicted in Fig. 4.

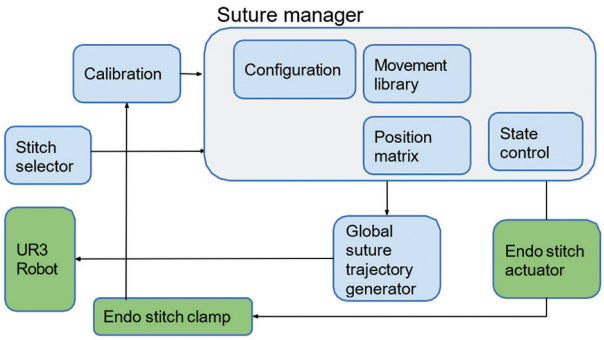

Fig. 4. System architecture for semi-automatic suturing

Fig. 4 presents a schematic diagram of the software control architecture developed for the robotic suturing system. This architecture, implemented on ROS (Robot Operating System), stands out for its modular design. The system's hardware components are identified in green: the collaborative "UR3 Robot," the motorized surgical "Endo stitch clamp," and the "Endo stitch actuator" responsible for actuating said clamp. These physical elements are integrated and managed by the software modules (represented in blue and light gray). The "Suture manager" acts as the cen-tral control core, orchestrating the operation. It receives inputs from the "Calibration" module (for spatial referencing) and the "Stitch selector" (to define the suturing task). Internally, the "Suture manager" contains the system "Configuration," the "Movement library" with movement primitives, the "Position matrix" which is used by the "Global suture trajectory generator" to plan the UR3 robot's trajectories and the "State control" which manages the operation sequence and commands the "Endo stitch actuator."

The main software modules include:

2.3.1. Configuration Module

This module allows configuring the system pa- rameters, including the suture characteristics: jaw closing speed, jaw opening percentage, distance between stitches, approach angle, the UR3 robot control parameters (e.g., maximum speeds and accelerations), and the type of stitch, which in the experiment is a continuous simple stitch.

2.3.2. Movement Library for Automated Suturing

This module implements a library of parameterized movements designed specifically for suturing tasks, ranging from the initial approach to thread tensioning. Each movement, defined in the joint space of the UR3 robot, is executed sequentially to perform a complete stitch. Fig. 5 graphically illustrates the functions that make up this library.

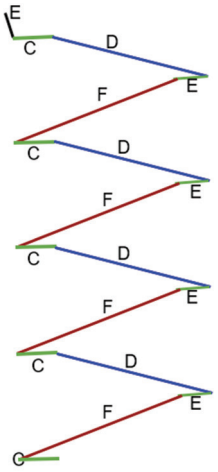

Fig. 5. Movement library for suturing

Trajectory (A) (in black) corresponds to the ini- tial approach to the suture area. Trajectory (B) (in green) represents the jaw change for the needle; before its execution, the jaws must be closed, ensuring secure needle holding through an inte- grated safety system. Trajectory (C) (in blue) is the thread extension movement, adjustable to dis- pense more thread in the first stitches and less in the last. Trajectory (D) (in black) represents the passage of the needle between the jaws, necessary depending on the type of suture used. Trajectory (E) (in red) represents the approach to the next stitch, a point from which the cycle repeats until the suture is complete. The arrangement of trajectories (B) in the graph symbolizes the different stitches needed to close the wound. It is essential to highlight that this pattern must be adapted to the specific morphology of the wound.

The implementation of this library of parameterized movements offers a modular and adaptable solution for different surgical scenarios. Breaking down the suturing process into a sequence of elementary and parameterizable movements facilitates the programming and adaptation of the robot to the specific geometry of the wound and the needs of the surgeon. This flexibility, combined with the integrated safety system to ensure secure needle holding, allows for optimizing the

precision and efficiency of the suturing process, minimizing inter-operator variability and potentially reducing surgical time, thereby improving clinical outcomes. Furthermore, the parameterization of the movements facilitates the incorporation of machine learning and adaptive control techniques, opening the door to the creation of autonomous suturing systems with the ability to adjust in real time to the changing conditions of the surgical environment.

2.3.3. Trajectory Planner

This module implements a trajectory planning algorithm based on the joint space of the UR3 robot, using cubic splines to generate smooth and continuous trajectories that avoid collisions and minimize execution time. The trajectory planner considers the speed and acceleration limitations of the UR3 robot and the EndoStitch forceps to ensure the safe and efficient operation of the system.

2.3.4. State Controller

This module manages the current state of the robotic system, including the position and orienta- tion of the UR3 robot, the state of the EndoStitch forceps (e.g., open, closed, passing the needle), and the progress of the suture. The state controller implements a state machine-based control logic that allows coordinating the execution of the different movements and tasks of the robotic system.

2.3.5. Calibration Module

This module implements a calibration proce- dure to align the coordinate system of the UR3 robot with the real workspace. This procedure is based on the identification of a set of reference points in the workspace, defined as the base of the robot. To do this, the robotic arm, equipped with the forceps, is sequentially moved to each calibration point. The corresponding Cartesian positions are recorded and then correlated with the desired positions of these points in the coordinate system of the UR3 robot. This correlation process allows for establishing a precise transformation be- tween the robot model and the physical environment, minimizing positioning errors and ensuring the accuracy of suturing tasks.

2.3.6. Robotic Suturing Protocol

The protocol for automated suturing, illustrated in Fig. 6, defines the integral workflow of the system, encompassing everything from the initial preparation of the surgical environment to the pre- cise execution of the stitches and the controlled completion of the process.

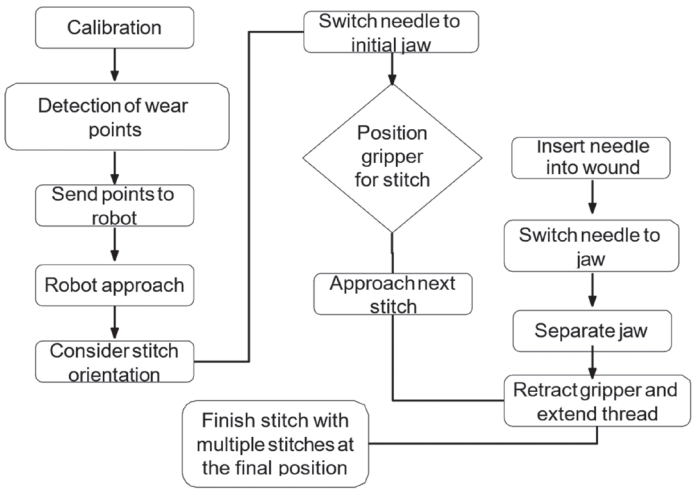

Fig. 6. Sequential diagram of the robotic suturing protocol

The protocol, designed to perform precise and reproducible sutures in various types of wounds, minimizing inter-operator variability and optimizing surgical time, is composed of the following stages:

Calibration and Wound Definition: This initial stage comprises system calibration, essential to align the robot's workspace with the physical reality. Next, key points that delimit the wound or the area to be sutured are detected, and defined by its shape and extension. Finally, the detected points are sent to the robot's control system, establishing the frame of reference for suturing.

Approach and Initial Preparation: In this phase, the robot makes an approach to the suture area, bringing the EndoStitch forceps to the starting point of the wound. At the same time, the desired orientation of the stitch is considered, adjusting the position of the forceps to ensure the correct penetration and direction of the needle in the tissue. In addition, the initial transfer of the needle is carried out, ensuring that it is correctly positioned in the initial jaw of the forceps.

Automated Suturing Cycle: This iterative stage comprises the repeated execution of the in- dividual stitch:

Positioning for the Stitch: It is evaluated whether it is necessary to position the gripper for the stitch.

Needle Insertion and Passage: The needle is inserted into the wound, passing through the tissue and completing the passage to the opposite jaw of the forceps (Needle Transfer).

Thread Extension and Tensioning: The forceps jaws are separated, extending the thread, while the robotic system retracts, extending and tensioning the thread, ensuring proper tissue closure.

Approach to the Next Stitch: The robot approaches the next stitch, preparing for needle insertion in the next position along the wound.

Suture Completion: After completing each cycle, it is decided whether it is the end of the process (Suture Completion). The repetition of the automated suturing cycle ceases when the desired number of stitches is reached, ensuring complete and effective closure of the wound with multiple stitches in the final position. This final stage could be considered as a knot to secure the suture.

2.4. EXPERIMENTAL EVALUATION ENVIRONMENT

The robotic suturing system was evaluated in a simulated environment using laparoscopic suturing training pads, model PH03-163, manufactured with soft silicone to simulate soft tissue. These pads, with dimensions of 14 x 14 x 1 cm and a weight of 181 g, were specifically designed for practicing basic laparoscopy skills. The silicone pad was fixed to a rigid base to simulate surgical tissue. The workstation was organized to ensure that all components of the system (UR3 robot, motorized EndoStitch forceps, control electronics, simulation pad) worked together efficiently, see 7 (b), (c). Constant and controlled lighting was main- tained to ensure correct visibility during the eval- uation. Fig. 7(a) presents the wounds selected for testing with the robot and forceps.

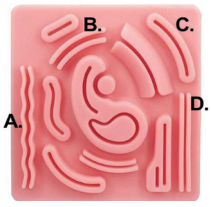

(a)

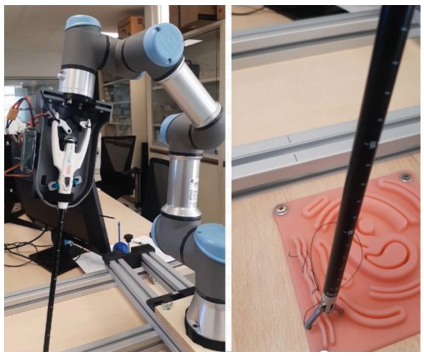

(b) (c)

Fig. 7. Experimental setup. (**a**). Suture pad used and wounds selected. (**b**) Robot forceps assembly. (**c**) Forceps on pad

The workflow is governed by a state machine whose activations and state changes allow the execution of stitch by stitch. Fig. 8 shows the evolution of a suture performed on wound type (a). The sequence can be observed through which the robot places the stitches on the wound until the suture is complete.

Fig. 8. Sequences of stitches on a wound

To have a margin for comparison of the experiments, a simulation was performed in Matlab where the robot develops the desired movement. In this case, it is observed how the robot is moving; the pattern shown in Fig. 9(a) represents the movement of separation of the wound to extend the thread. In Figs. 9(b), (c), the robot is shown developing the desired trajectory.

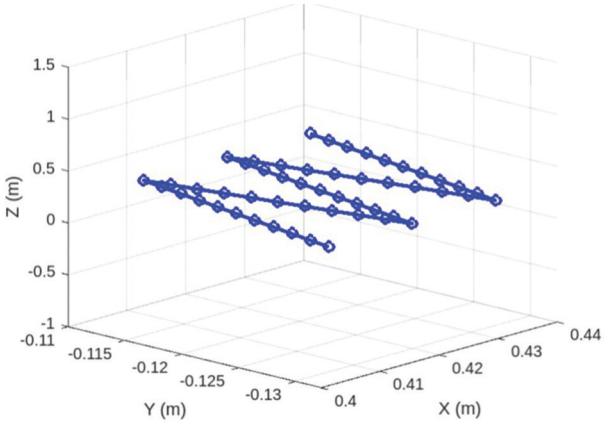

(a)

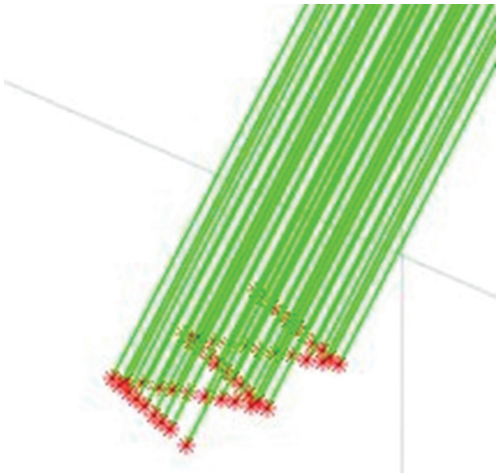

(b)

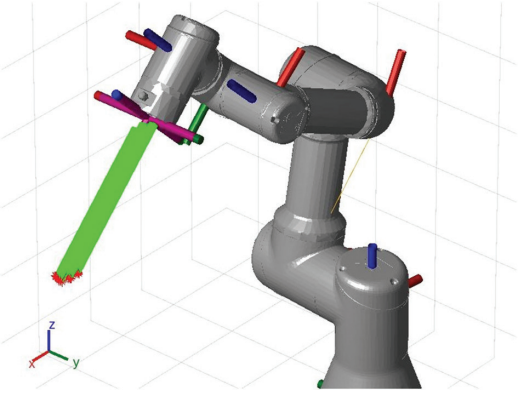

(c)

Fig. 9. Simulation. (**a**) Desired trajectory, (**b**) Achieved trajectory, (**c**) Robot movement

The results of the simulated desired trajectory are shown in Fig. 10. As expected, the simulated error was significantly smaller—on the order of nanometers.

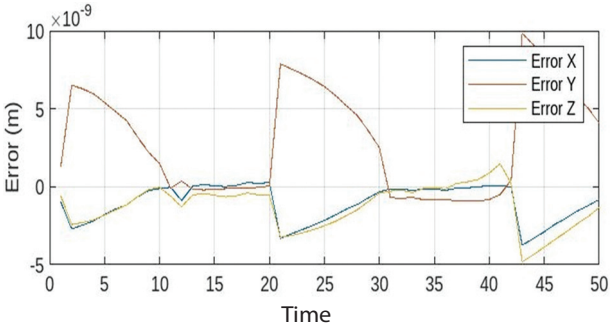

Fig. 10. Error obtained in the simulation

It can be observed that the errors in the X and Y axes are nearly identical, while the error in the Z-axis exhibits some noticeable peaks, indicating a different behavior.

3. RESULTS

This section presents the results of an experiment designed to evaluate the accuracy of a semiautonomous robotic system in performing surgical sutures. The experiment consisted of performing four independent suturing tests on different wounds present on the test pad using a motorized EndoStitch forceps integrated with the UR3 robotic arm. The main objective was to quantify the positioning error of the system in the three dimensions during the suturing process. In each test, the robot performed a series of stitches in the simulated tissue, and the deviation between the desired position and the actual position of the needle was measured in each stitch. (The table shows the experimental data 2)

Table 2. Statistical Summary of Positioning Error by Test Configuration ($N = 6$ per test)

Test	Axis	Mean (x^-) ($\times 10^{-5}$ m)	Std. Dev. (s) ($\times 10^{-5}$ m)	95% CI ($\times 10^{-5}$ m)	CV (%)
*A	X	0.9	0.25	[0.64, 1.16]	27.8
	Y	0.8	0.20	[0.59, 1.01]	25.0
	Z	1.6	0.55	[1.02, 2.18]	34.4
*B	X	1.1	0.40	[0.68, 1.52]	36.4
	Y	1.0	0.35	[0.63, 1.37]	35.0
	Z	1.2	0.45	[0.73, 1.67]	37.5
*C	X	2.0	0.70	[1.27, 2.73]	35.0
	Y	0.9	0.25	[0.64, 1.16]	27.8
	Z	1.7	0.60	[1.08, 2.32]	35.3
*D	X	0.6	0.15	[0.44, 0.76]	25.0
	Y	0.5	0.10	[0.39, 0.61]	20.0
	Z	0.7	0.20	[0.49, 0.91]	28.6

CI: Confidence Interval; CV: Coefficient of Variation; $t_{0.025,5} = 2.571$

3.1. STATISTICAL SUMMARY OF POSITIONING ACCURACY

The experimental design employed $N = 6$ independent repetitions for each test configuration, totaling 24 trials across four wound geometries.

This sample size was determined based on statistical power analysis to detect meaningful differences in positioning accuracy while maintaining practical experimental constraints.

For precision measurements in robotic systems, $N = 6$ provides sufficient statistical power ($\beta > 0.80$) to detect effect sizes of practical signifi- cance ($\delta \geq 0.5 \times 10^{-5}$ m) with $\alpha = 0.05$. The sample size ensures reliable estimation of population parameters while accounting for the controlled experimental environment and high precision instrumentation that minimizes measurement variability.

The statistical analysis demonstrates high system reliability, with positioning accuracy consis- tently in the 10^{-5} meter range across all configurations. The mean positioning errors range from 0.5×10^{-5} m (Test D, Y-axis) to 2.0×10^{-5} m (Test C, X-axis), representing a 200-fold improvement over manual suturing precision ($\sim 2 \times 10^{-3}$ m). Standard deviations remain below 0.70×10^{-5} m in all cases, indicating consistent performance across repetitions.

The 95% confidence intervals provide statisti- cal assurance of system performance bounds un- der operational conditions. Coefficients of vari- ation (CV) rang-

ing from 20.0 % to 37.5 % reflect the inherent variability in complex robotic systems while maintaining clinically acceptable precision levels. The narrow confidence intervals, particularly for Test D (straight geometry), confirm that the proposed system achieves reproducible submillimetric accuracy suitable for precision surgical applications.

The statistical robustness of $N = 6$ repetitions is validated by the tight confidence bounds and consistent CV values, providing sufficient evidence for the system's reliability and establishing a foun- dation for clinical translation studies with larger sample sizes.

The main evaluation metric was the positioning error, defined as the vector distance between the target position of the needle and its actual position after insertion. This error was decomposed into three components: error in the X component (lat- eral), error in the Y component (depth), and error in the Z component (vertical). The results of each test are presented in Figs.11 and 12, where the error in the three components is plotted for each stitch performed. The analysis of these results allowed identifying characteristic error patterns of the system, as well as the variability of the performance between the different tests.

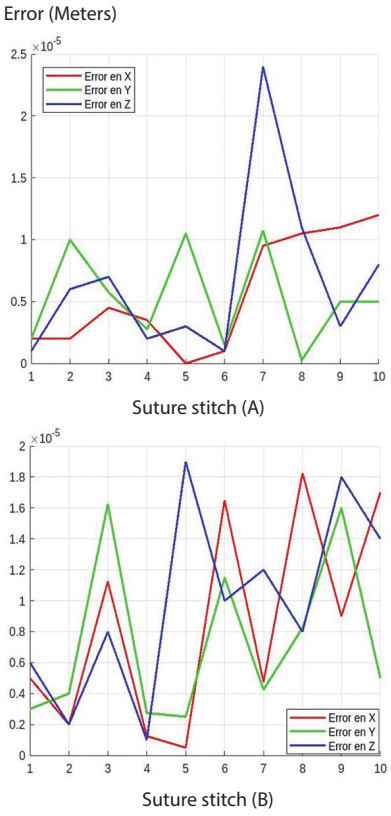

Fig. 11. Experimental results of the tests on wound types A and B, the corresponding wounds are those shown in Figure 7(a).

Figs. 11 and 12 illustrate the results of four independent robotic suturing tests (a, b, c, d) conducted on tissue simulators, displaying the positioning error (in meters) for each stitch across the X (red), Y (green), and Z (blue) components. The horizontal axis represents the stitch number, while the vertical axis indicates the error magnitude. The tests were performed using a semi-autonomous robotic system based on ROS, employing a latex training pad with simulated wounds: test (a) corresponds to a straight but sinusoidal wound, and test

(b) to a slightly curved arc-shaped wound, both featuring a groove that enhances the edges. Target positions were predefined and stored using the same robot, with no modifications to the control architecture between tests, allowing the evaluation of the influence of wound geometry and tissue orien- tation on the system's accuracy.

DETAILED ANALYSIS BY TEST

Test (A): Sinusoidal Wound

In the sinusoidal wound test, the positioning error in the X and Y directions remains generally stable, with values below 1.5×10^{-5} meters, whereas a significant peak of approximately 2.4×10^{-5} meters is observed in the Z component at stitch 7. This increase may be attributed to the sinusoidal geometry, which introduces rapid changes in tissue orientation at the groove's inflection points. In these regions, the interaction between the EndoStitch forceps and the latex surface likely complicates precise control of needle insertion depth (Z) due to variations in material resistance or deformation. The upward trend in X error from stitch 6 suggests a progressive accumulation of inaccuracies while following the curved trajectory, possibly amplified by propagated errors in the horizontal plane. In contrast, the Y error remains more contained, though it exhibits a peak at stitch 2 (with no immediately apparent cause), indicating relatively stable control in the direction of advancement, but with potential limitations in compensating for the sinusoidal curvature within the planned trajectory.

Test (B): Slightly Curved Parallel Wound

In the slightly curved wound test, errors across all three components (X, Y, Z) show greater vari- ability, ranging between 0.2×10^{-5} and 1.8×10^{-5} meters, with notable peaks at stitches 2, 5, and 8. The arc-shaped curvature, though mild, introduces additional complexity to positioning control, requiring continuous trajectory adjustments by the UR3 robot. The alternating peaks across components suggest that the system struggles to coordinate movements between axes while adapting to the curve, potentially exacerbating inherent instabilities or inter-axis interactions. Furthermore, the curvature may induce subtle variations in the ten- sion of the simulated tissue along the groove, affecting needle insertion and contributing to error dispersion. The absence of dynamic adjustments in the control architecture between tests indicates that the system was not optimized for this geometry, allowing small initial errors to propagate and amplify along the trajectory, particularly in the Z direction, where maintaining needle perpendicularity to the groove is more challenging.

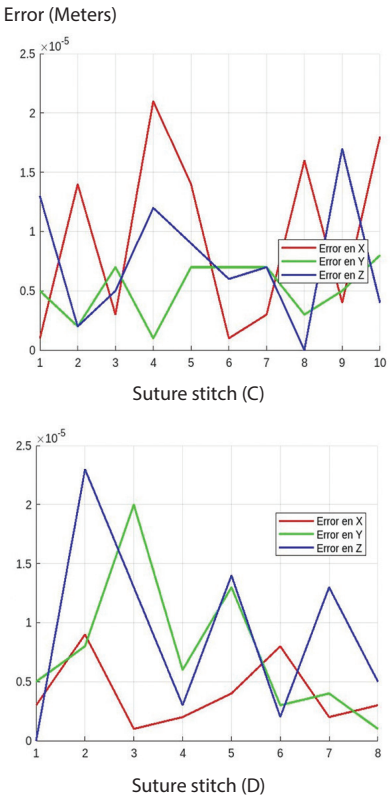

Fig. 12. Experimental results of the tests on wound types C, D. The corresponding wounds are those shown in Figure 7(a).

Test (C): Non-Parallel Curved Wound

In test (c), the error in the X component (red) stands out with a higher magnitude, reaching peaks of up to 2.5×10^{-5} meters at stitches 2, 4, and 8, while Y (green) remains stable ($< 1.5 \times 10^{-5}$ m) and Z (blue) fluctuates with a peak at stitch 2 ($\sim 2.0 \times 10^{-5}$ m). This is due to the arc geometry in the opposite direction to test (b), requiring constant adjustments in the EndoStitch forceps orientation to follow the curved groove. The nonparallel alignment with the UR3 robot's axes misaligns the X-axis with the main suturing direction, leading to cumulative lateral deviations. The stability in Y suggests effective transverse control, but Z fluctuations indicate challenges in maintaining uniform needle depth amid changing tissue orientation. A possible justification is that the ROSbased control architecture, lacking dynamic adjustments, fails to adequately compensate for the multi-axis complexity of the reversed curve, allowing small initial inaccuracies to amplify, particularly in X, where reorientation is most critical.

Test (D): Narrow Straight Wound

In test (d), initial errors in Y (green) and Z (blue) are higher, peaking at stitch 2 ($\sim 2.0 \times 10^{-5}$ m), while X (red) remains low. From stitch 4 onward, all three components converge to consistent values ($< 1.0 \times 10^{-5}$ m), indicating stabilization. The straight trajectory facilitates predictable tracking, reducing variability after the initial stitches. The early Z peak may stem from a specific interaction between the forceps and the uniform-height groove in the latex pad, such as local deformation or suboptimal motion parameterization, while the Y error suggests an initial transverse calibration issue. The likely justification is that the linear simplicity allows the system to quickly adapt after a brief settling period, and the groove's uniformity minimizes external factors, though unmeasured forces prevent confirming whether material resistance contributed to the Z peak.

The greater variability in (c) is justified by the complexity of the reversed curvature, demanding multi-axis coordination that the static control system cannot optimize, resulting in accumulated X errors. In (d), stability after initial stitches is explained by the ease of following a straight path, enabling the robot to correct early inaccuracies and leverage geometric predictability. Z peaks in both tests may be justified by latex interaction (resistance or deformation), unaddressed by the static control, while Y stability in (c) and convergence in (d) reflect the system's ability to handle directions less affected by specific geometry.

It is important to note that, despite this variability in the error pattern, the magnitude of the positioning error consistently remains in the order of micrometers. Although there are specific peaks that reach tens of micrometers, the overall error scale is in this micrometric range. This precision, even considering the variability, represents a level of accuracy on the order of magnitude of the typical accuracy of manual suturing performed by experienced surgeons (approximately 2 mm). This difference suggests that, despite the variability observed in the different test conditions, the robotic system has the potential to offer a notably improved positioning accuracy in the suturing task compared to manual execution.

4. DISCUSSION

The results of this study, although promising, reveal critical aspects for the successful development of robotic suturing systems. The variability observed in the positioning error between tests, even with a micrometric magnitude, underscores the need for robust and adaptable control that can compensate for disturbances and uncertainties present in the real surgical environment. While the error in the simulation reached nanometric levels, this difference highlights the inherent complexity of the real environment compared to the simplified models used in simulation. However, the identification of similar patterns in the error peaks between the simulation and the experiments suggests that the model captures fundamental elements of the system, validating its usefulness in optimizing the design and control strategies. This observation is crucial, as it implies that the simulation can be a valuable tool to predict and mitigate certain types of errors before conducting tests in more complex and costly environments.

The implementation of a parameterized movement library, along with the strategic choice of the UR3 robot

and the motorized EndoStitch forceps, proved to be suitable options for the research. However, it is imperative to recognize the limitations inherent in the evaluation in a simulated environment. The complexity of living tissue, with its viscoelastic properties and dynamic behavior, is not fully replicated in the simulation pads. Therefore, a more thorough statistical analysis, including a greater number of repetitions and the evaluation of the statistical significance of the observed differences, along with tests in more realistic models (such as animal tissues or biomimetic models), are essential steps for a complete and robust evaluation of the system. This more rigorous evaluation will allow determining more precisely the real potential of the robotic system in a clinical surgical environment.

In comparison with the work of [11], this study focuses on the automation of a different forceps. However, instead of considering them as mutually exclusive solutions, the possibility of a strategic coexistence could be explored. Integrating the advantages of both automated forceps could lead to a more versatile and adaptable system. For example, the EndoStitch Forceps, with its larger bite, could be more efficient for tasks such as anastomosis and tissue coaptation, where precise joining or approximation of large areas of tissue is required. In contrast, the other forceps could be more suitable for tasks that demand greater precision in confined spaces.

Unlike grasper-based approaches such as Endowrist or Endo360, where needle re-grasping poses a significant technical challenge, our solution with the motorized EndoStitch leverages its inherently and clinically validated capability for automatic needle transfer. This distinctive feature drastically simplifies robotic control during this critical phase, enhancing the reliability of needle handling and allowing the system to focus on precise positioning. Potentially, this translates into more consistent and uniform suturing, a possible reduction in the surgical time devoted to suturing, and a lower cognitive load for the surgeon, with the potential to improve therapeutic outcomes by enabling smoother and more efficient automated procedures.

The simulation analysis reveals a contact interaction. This value, although indicative of the internal load, differs from the high reaction forces (e.g., 26-30 N by [22], 0-40 N/m by [23]) reported in the literature for needle insertion. This discrepancy can be attributed to the rigid boundary conditions of the current simulation and the absence of a tissue damage model, factors that tend to artificially increase the penetration resistance in the model compared to ex vivo experimental scenarios where the tissue can deform or tear, reducing the forces and local stress.

Despite these limitations, stress analysis offers significant advantages over simple force measurement. It allows for the prediction of material failure or deformation by comparing the calculated stress with the material's intrinsic limits, the identification of critical points through the visualization of stress concentrations (crucial for the design of sharp tools), and the optimization of designs for efficiency and safety. Unlike total force, stress provides a detailed understanding of how the load is distributed internally, offering deeper insight into contact mechanics and its impact on the material. For future research, and to better align the results with clinical reality, it is essential to incorporate more complex material models that reflect tissue anisotropy and heterogeneity, as well as damage or fracture models.

5. CONCLUSION

This study successfully developed and evaluated a semi-autonomous robotic system for the automation of surgical suturing, integrating a motorized EndoStitch forceps with a UR3 robot and a ROS-based control architecture. The system demonstrated significant precision in performing suturing tasks on simulated tissue.

The quantitative evaluation of the system's positioning accuracy revealed promising results. Across four different simulated wound geometries and with N=6 repetitions per test, mean positioning errors were consistently maintained in the micrometer range. Specifically, mean errors along the X, Y, and Z axes ranged from as low as 0.5×10^{-5} m (Test D, Y-axis) to a maximum of 2.0×10^{-5} m (Test C, X-axis), as detailed in Table 2. Standard deviations remained consistently low, with the highest recorded at 0.70×10^{-5} m, indicating repeatable performance. This level of precision represents a substantial, approximately 200-fold improvement over typical manual suturing accuracy (estimated around 2×10^{-3} m).

While the overall performance achieved micrometer-level accuracy, the analysis also highlighted variability influenced by wound geometry. For instance, Test C (non-parallel curved wound) exhibited peak errors in the X-component up to 2.5×10^{-5} m. Coefficients of Variation (CV) across all tests and axes ranged from 20.0% to 37.5%, reflecting the inherent complexities of robotic interaction with deformable surfaces and the current control strategy. Despite this variability, the achieved precision, even at its observed peaks, remains orders of magnitude better than manual execution.

These findings validate the feasibility of the developed system for automated suturing and underscore its potential to significantly enhance precision and consistency compared to manual techniques. The obtained quantitative data provide a strong baseline and highlight that while micrometer accuracy is achievable, future work should focus on optimizing control algorithms to further reduce error variability, particularly in response to complex tissue interactions and wound paths. Further evaluation in more realistic biological models and eventually in clinical settings, alongside the development of adaptive control strategies, possibly incorporating machine learning, will be crucial for translating this promising technology into tangible clinical benefits, such as reduced surgeon cognitive load and improved patient outcomes.

6. REFERENCES

[1] E. Lau, N. A. Alkhamesi, C. M. Schlachta, "Impact of robotic assistance on mental workload and cognitive performance of surgical trainees performing a complex minimally invasive suturing task", Surgical Endoscopy, Vol. 34, No. 6, 2020, pp. 2551-2559.

[2] F. Ju, X. Luo, L. Ding, "Multifunctional Robotic Surgical Forceps With Tactile Sensor Array for Tissue Palpation and Clamping Status Detection", IEEE Sensors Journal, Vol. 24, No. 10, 2024, pp. 16883-16891.

[3] Y. Yamasaki et al. "Effects of a force feedback function in a surgical robot on the suturing procedure", Surgical Endoscopy, Vol. 38, No. 3, 2024, pp. 1222-1229.

[4] K. Wang, J.-N. Ma, C.-Y. Zhang, Z. Pei, W.-T. Tang, Q. Zhang, "Self-powered high-sensitivity piezoelectric sensors for end-fixture force sensing in surgical robots based on T-ZnO", Colloids and Surfaces A: Physicochemical and Engineering Aspects, Vol. 697, 2024, p. 134424.

[5] Z. Cheng, M. Chauhan, B. L. Davies, D. G. Caldwell, L. S. Mattos, "Modelling needle forces during insertion into soft tissue", Proceedings of the Annual International Conference of the IEEE Engineering in Medicine and Biology Society, Milan, Italy, 25-29 August 2015, pp. 4840-4844.

[6] Y. Zhang, F. Ju, X. Wei, D. Wang, Y. Wang, "A Piezoelectric Tactile Sensor for Tissue Stiffness Detection with Arbitrary Contact Angle", Sensors, Vol. 20, No. 22, 2020, p. 6607.

[7] C.-H. Yeh et al. "Application of piezoelectric actuator to simplified haptic feedback system", Sensors and Actuators A: Physical, Vol. 303, 2020, p. 111820.

[8] T. Gopel, F. Hartl, A. Schneider, M. Buss, H. Feussner, "Automation of a suturing device for minimally invasive surgery", Surgical Endoscopy, Vol. 25, No. 7, 2011, pp. 2100-2104.

[9] Y. Hu, W. Li, L. Zhang, G.-Z. Yang, "Designing, Prototyping, and Testing a Flexible Suturing Robot for Transanal Endoscopic Microsurgery", IEEE Robotics and Automation Letters, Vol. 4, No. 2, 2019, pp. 1669-1675.

[10] S. N. Kurenov, S. Punak, M. Kim, J. Peters, J. C. Cendan, "Simulation for training with the autosuture endo stitch device", Surgical Innovation, Vol. 13, No. 4, 2006, pp. 283-287.

[11] H. Saeidi, H. Le, J. D. Opfermann, S. Leonard, A. Kim, M. H. Hsieh, J. U. Kang, A. Krieger, "Autonomous Laparoscopic Robotic Suturing with a Novel Actuated Suturing Tool and 3D Endoscope", Proceedings of the International Conference on Robotics and Automation, Montreal, QC, Canada, 20-24 May 2019, pp. 1541-1547.

[12] S. A. Pedram, P. Ferguson, J. Ma, E. P. Dutson, J. Rosen, "Optimal needle diameter, shape, and path in autonomous suturing", arXiv:1901.04588, 2019.

[13] J. Colan, J. Nakanishi, T. Aoyama, Y. Hasegawa, "Optimization-based constrained trajectory generation for robot-assisted stitching in endonasal surgery", Robotics, Vol. 10, No. 1, 2021.

[14] S. A. Pedram, C. Shin, P. W. Ferguson, J. Ma, E. P. Dutson, J. Rosen, "Autonomous Suturing Framework and Quantification Using a Cable-Driven Surgical Robot", IEEE Transactions on Robotics, Vol. 37, No. 2, 2021, pp. 404-417.

[15] Y. Tian, M. Draelos, G. Tang, R. Qian, A. N. Kuo, J. A. Izatt, K. Hauser, "Toward Autonomous Robotic Micro-Suturing using Optical Coherence Tomography Calibration and Path Planning", Proceedings of the IEEE International Conference on Robotics and Automation, Paris, France, 2020, pp. 5516-5522.

[16] A. E. Abdelaal, J. Liu, N. Hong, G. D. Hager, S. E. Salcudean, "Parallelism in Autonomous Robotic Surgery", IEEE Robotics and Automation Letters, Vol. 6, No. 2, 2021, pp. 1824-1831.

[17] H. Dehghani, Y. Sun, L. Cubrich, D. Oleynikov, S. Farritor, B. Terry, "An Optimization-Based Algorithm for Trajectory Planning of an Under-actuated Robotic Arm to Perform Autonomous Suturing", IEEE Transactions on Biomedical Engineering, Vol. 68, No. 4, 2021, pp. 1262-1272.

[18] S. Gao, S. Ji, M. Feng, X. Lu, W. Tong, "A study on autonomous suturing task assignment in robot-assisted minimally invasive surgery", The International Journal of Medical Robotics + Computer Assisted Surgery: MRCAS, Vol. 17, No. 1, 2021.

[19] H. Vargas, V. Munoz, A. Vivas, "Automated suturing: sharp wound recognition and planning with surgical robot", Advanced Robotics, Vol. 37, No. 14, 2023, pp. 900-917.

[20] O. L. T. Diaz, J. L. C. Gonzalez, O. A. V. Alban, J. C. F. Marinero, "Design, simulation and first test of an automatic suturing device coupled to a robot", Reveia, Vol. 21, No. 41, 2024, pp. 1-18.

[21] G. H. Mahmud, Z. Yang, A. M. T. Hassan, "Experimental and numerical studies of size effects of Ultra High Performance Steel Fibre Reinforced Concrete (UHPFRC) beams", Construction and Building Materials, Vol. 48, 2013, pp. 1027-1034.

[22] Y. Jiang, Q. Song, X. Luo, "3D Cohesive Finite Element Minimum Invasive Surgery Simulation Based on Kelvin-Voigt Model", Chinese Journal of Mechanical Engineering, Vol. 35, No. 1, 2022.

[23] M. Terzano, D. Dini, F. R. y Baena, A. Spagnoli, M. Oldfield, "An adaptive finite element model for steerable needles", Biomechanics and Modeling in Mechanobiology, Vol. 19, No. 5, 2020, pp. 1809-1825.